a mimic of the smaller functional epitope may suffice. Our findings suggest starting points for these design strategies.

REFERENCES AND NOTES

1. J. Janin and C. Chothia, *J. Biol. Chem.* **265**, 16027 (1990).
2. D. R. Davies, E. A. Padlan, S. Sheriff, *Annu. Rev. Biochem.* **59**, 439 (1990); I. A. Wilson and R. L. Stanfield, *Curr. Opin. Struct. Biol.* **3**, 113 (1993).
3. A. M. de Vos, M. Ultsch, A. A. Kossiakoff, *Science* **255**, 306 (1992).
4. G. Fuh *et al.*, *ibid.* **256**, 1677 (1992); B. C. Cunningham, P. Jhurani, P. Ng, J. A. Wells, *ibid.* **243**, 1330 (1989). For review, see J. A. Wells *et al.*, *Recent Prog. Horm. Res.* **48**, 253 (1993).
5. The values of $(\Delta\Delta G)_{mut\text{-}wt}$ were calculated as $+RT\ln(K_d \text{ mutant}/K_d \text{ wild type})$, where R is the gas constant and T is the absolute temperature.
6. Our analysis is based on a crystal structure of the 1:1 complex at 2.6 Å resolution [A. M. de Vos and M. Ultsch, in preparation]. Compared with the 2:1 structure at 2.8 Å resolution that included a second receptor (*3*), the 1:1 structure shows the previously disordered loop region T73 to E75 in the hGHbp and many ordered water molecules. In other respects the interface is essentially unchanged, except that the flexible COOH-terminus of hGH makes different contacts (with receptor residues T194 and T195).
7. Solvent accessibilities were calculated with a rolling sphere of radius 1.4 Å [B. K. Lee and F. M. Richards, *J. Mol. Biol.* **55**, 379 (1971)].
8. Amino acids are denoted with the one-letter code as follows: A, Ala; C, Cys; D, Asp; E, Glu; F, Phe; G, Gly; H, His; I, Ile; K, Lys; L, Leu; M, Met; N, Asn; P, Pro; Q, Gln; R, Arg; S, Ser; T, Thr; V, Val; W, Trp; and Y, Tyr. Mutants are designated by the wild-type residue, followed by its position, and the mutant residue.
9. B. C. Cunningham and J. A. Wells, *Science* **244**, 1081 (1989). For review, see J. A. Wells, *Methods Enzymol.* **202**, 390 (1991).
10. S. H. Bass, M. G. Mulkerrin, J. A. Wells, *Proc. Natl. Acad. Sci. U.S.A.* **88**, 4498 (1991).
11. Most mutants were engineered, expressed in *E. coli*, and purified by hGH affinity chromatography essentially as described [(*10*); G. Fuh *et al.*, *J. Biol. Chem.* **265**, 3111 (1990)]. Some mutants had been constructed previously (*10*). Mutants W104A, P106A, and W169A were purified by ion-exchange chromatography and hydrophobic interaction chromatography on a BIOcad workstation (Perseptive Biosystems). Binding affinities for hGH were determined by competitive displacement with ^{125}I-labeled hGH as the tracer [S. A. Spencer *et al.*, *ibid.* **263**, 7862 (1988)] except that monoclonal antibody (mAb) 5 [R. Barnard, P. G. Bundesen, D. B. Rylatt, M. J. Waters, *Endocrinology* **115**, 1805 (1984)] was used to precipitate hGH-hGHbp complexes. This mAb blocks dimerization of hGHbp [B. C. Cunningham *et al.*, *Science* **254**, 821 (1991)] so that simple 1:1 binding affinity can be accurately determined. Any discrepancies between the present data and other measurements of affinities (*10*) can be ascribed to the previous use of mAb 263, which does not block dimerization.
12. The affinities of W104A and W169A were below the sensitivity of the assay ($K_d > 1$ μM), which is fixed by the availability of mAb 5 for precipitation. We estimated the affinity of these mutants for hGH to be 1/2500 that of the wild-type hGHbp protein or even lower. The mutations do not appear to introduce global structural disruptions into hGHbp, as their reactivities with a panel of mAbs were unchanged [(*10*); T. Clackson and J. A. Wells, unpublished data]; in addition, the W104A mutant has a native-like circular dichroism spectrum (*10*) and can bind to a variant of hGH engineered to have higher receptor-binding affinity [H. B. Lowman and J. A. Wells, *J. Mol. Biol.* **234**, 564 (1993); S. Atwell and J. A. Wells, unpublished data].
13. The sum of the apparent binding free energy contributions of each interface residue (≤ -27 kcal/mol) considerably exceeds the known binding free energy for the complex (−12.3 kcal/mol). This implies that some of the mutations we engineered are not having independent effects. This can be explained by the fact that many of these side chains make intramolecular contacts [for a discussion, see J. A. Wells, *Biochemistry* **29**, 8509 (1990)].
14. B. C. Cunningham and J. A. Wells, *J. Mol. Biol.* **234**, 554 (1993).
15. C. Chothia, *Nature* **254**, 101 (1974).
16. ——— and J. Janin, *ibid.* **256**, 705 (1975).
17. R. L. Stanfield, T. M. Fieser, R. A. Lerner, I. A. Wilson, *Science* **248**, 712 (1990).
18. R. E. Hawkins, S. J. Russell, M. Baier, G. Winter, *J. Mol. Biol.* **234**, 958 (1993).
19. W. R. Tulip, V. R. Harley, R. G. Webster, J. Novotny, *Biochemistry* **33**, 7986 (1994).
20. D. Eisenberg and A. D. McLachlan, *Nature* **319**, 199 (1986); N. Horton and M. Lewis, *Protein Sci.* **1**, 169 (1992); J. A. Wells, unpublished observations.
21. T. N. Bhat *et al.*, *Proc. Natl. Acad. Sci. U.S.A.* **91**, 1089 (1994).
22. A. M. Buckle, G. Schrieber, A. R. Fersht, *Biochemistry* **33**, 8878 (1994).
23. F. A. Quiocho *et al.*, *Nature* **340**, 404 (1989).
24. Z. Otwinowski *et al.*, *ibid.* **335**, 321 (1988).
25. R. F. Kelley and M. P. O'Connell, *Biochemistry* **32**, 6828 (1993).
26. L. Jin, B. M. Fendly, J. A. Wells, *J. Mol. Biol.* **226**, 851 (1992); J. M. Nuss, P. B. Whitaker, G. M. Air, *Proteins Struct. Funct. Genet.* **15**, 121 (1993).
27. J. Novotny, R. E. Bruccoleri, F. A. Saul, *Biochemistry* **28**, 4735 (1989).
28. L. Young *et al.*, *Protein Sci.* **3**, 717 (1994).
29. B. C. Cunningham and J. A. Wells, *Proc. Natl. Acad. Sci. U.S.A.* **88**, 3407 (1991).
30. W. S. Somers, M. H. Ultsch, A. M. de Vos, A. A. Kossiakoff, *Nature* **372**, 478 (1994).
31. P. Argos, *Protein Eng.* **2**, 101 (1988).
32. D. W. Banner *et al.*, *Cell* **73**, 431 (1993).
33. T. E. Ferrin, C. L. Huang, L. E. Jarvis, R. Langridge, *J. Mol. Graph.* **6**, 13 (1988).

34. We thank A. de Vos for sharing unpublished crystallographic data and for many helpful discussions; S. Bass, B. Cunningham, G. Fuh, and D. Matthews for reagents and advice; W. Anstine and K. Andow for assistance with preparing graphics; and the oligonucleotide synthesis and fermentation groups at Genentech. T.C. was supported in part by a North Atlantic Treaty Organization postdoctoral fellowship.

15 September 1994; accepted 13 December 1994

Solution Structure of the Epithelial Cadherin Domain Responsible for Selective Cell Adhesion

Michael Overduin, Timothy S. Harvey, Stefan Bagby, Kit I. Tong, Patrick Yau, Masatoshi Takeichi, Mitsuhiko Ikura*

Cadherins are calcium-dependent cell adhesion molecules containing extracellular repeats of approximately 110 amino acids. The three-dimensional structure of the amino-terminal repeat of mouse epithelial cadherin was determined by multidimensional heteronuclear magnetic resonance spectroscopy. The calcium ion was bound by a short α helix and by loops at one end of the seven-stranded β-barrel structure. An exposed concave face is in a position to provide homophilic binding specificity and was also sensitive to calcium ligation. Unexpected structural similarities with the immunoglobulin fold suggest an evolutionary relation between calcium-dependent and calcium-independent cell adhesion molecules.

Selective interactions between cells that lead to morphogenesis require the action of cell adhesion molecules (CAMs). The cadherin and immunoglobulin (Ig) CAM superfamilies provide Ca^{2+}-dependent and Ca^{2+}-independent cell adhesion, respectively (*1*). Most vertebrate and some invertebrate cells express at least one cadherin and require Ca^{2+} to form solid tissues. Loss of epithelial cadherin (E-cadherin) expression is correlated with the invasive potential of tumor cells (*2*). The 30 known cadherins typically contain five extracellular repeats (here termed CAD repeats), a single membrane-spanning region, and a cytoplasmic region. The NH_2-terminal CAD (CAD1) repeat is essential for the homophilic binding specificity that directs "like" cadherins to associate (*3*). The cytoplasmic region of E-cadherin (also called uvomorulin) is anchored to cytoskeletal actin microfilaments through catenins (*4*). Here we present the solution structure of the CAD1 domain of E-cadherin spanning amino acids 1 through 104 (referred to hereafter as E-CAD1), determined in the presence of Ca^{2+} from 1793 nuclear magnetic resonance (NMR)–derived structural restraints (*5*).

The structure of E-CAD1 contains seven β strands (βA through βG) and two short α helices (αA and αB) (Fig. 1A). All β strand pairings are antiparallel except for that between βA′ and βG, with a β-barrel topology similar to that of the Ig constant (C) domain (*6*). Bulges in βB and βG contribute to the curling of the β sheet into a barrel shape (Fig. 1B). A proline-proline junction between βA and βA′ bridges the two ends of the sheet. Despite its helical appearance, the backbone dihedral angles in the CD loop are not compatible with a helix. The DE and FG junctions are β hairpin turns. Conservation of the β-barrel fold of E-CAD1 among other CAD repeats is evident from the alignment of structurally critical proline, glycine, and

M. Overduin, T. S. Harvey, S. Bagby, K. I. Tong, P. Yau, M. Ikura, Division of Molecular and Structural Biology, Ontario Cancer Institute, and Department of Medical Biophysics, University of Toronto, 500 Sherbourne Street, Toronto, Ontario, Canada, M4X 1K9.
M. Takeichi, Department of Biophysics, Faculty of Science, Kyoto University, Kitashirakawa, Sakyo-ku, Kyoto 606, Japan.

*To whom correspondence should be addressed.

buried hydrophobic residues (Fig. 1C). The length and spacing of the secondary structure elements are also conserved, which indicates that additional β strands are unlikely to be inserted into the β barrels of other CAD domains.

The homophilic binding specificity of cadherins appears to be governed by their CAD1 domains through a surface that includes the HAV (*7*) motif. Cell adhesion mediated by E-cadherin has been shown to be inhibited by peptides containing this motif (*8*). Partial specificity for placental cadherin (P-cadherin) can be conferred on E-cadherin by Ser^{78}→Gly^{78} and Ser^{83}→Glu^{83} mutations that border the HAV motif (*3*). The His^{79}-Ala-Val sequence, Ser^{78}, and Ser^{83} are found in or following βF of the E-CAD1 structure (Fig. 1A). Additional elements must contribute to homophilic binding specificity, because the conversion of specificity due to the two point mutations was only partial. We propose that the concave βCFG surface of CAD1 domains provides cadherins with homophilic specificity. Solvent-exposed amino acids on this surface include Lys^{33} preceding βC, Phe^{35} and Ser^{37} in βC, His^{79} and Val^{81} in βF, Ser^{83}-Gly^{85} in GF, and Glu^{86}-Pro^{91} in βG. The analogous βCFG face of CD2, a T cell–specific CAM of the Ig superfamily (*9*), interacts with CD58 (*10*). Although the binding partners of CAD1 domains have not yet been established, the monomeric state indicated by NMR and other studies of the cadherin polypeptide (*5*) suggests that E-CAD1 binds to an E-CAD domain other than itself through this βCFG surface.

The Ca^{2+} binding site of E-CAD1 was inferred by identification of amino acid residues whose backbone ^{13}CO, ^{15}N, or ^{1}HN chemical shifts differed between Ca^{2+}-bound and Ca^{2+}-free forms (Fig. 2A). Chemical shift changes indicate structural or dynamic perturbations expected from such interactions. The three elements in E-CAD1 exhibiting the most chemical shift changes are Pro^{10}-Glu-Asn-Glu in the AB loop, Leu^{66}-Asp-Arg-Glu in αB, and the Asp^{100}-Gln-Asn-Asp sequence following βG. A negatively charged pocket is formed by these three elements with the side chains of the highly conserved Glu^{11}, Glu^{69}, and Asp^{100} well positioned to ligate Ca^{2+} (Fig. 2B).

The proposed homophilic specificity surface is also sensitive to Ca^{2+} ligation. In particular, His^{79} and the juxtaposed Met^{92} display large chemical shift changes on addition of Ca^{2+} (Fig. 2A). These effects do not suggest a second Ca^{2+} binding site because no negatively charged residues in this region were found to exhibit substantial Ca^{2+}-induced chemical shift changes. Rather, they likely represent an indirect effect of Ca^{2+} ligation in a pocket 20 Å away. This Ca^{2+}-induced conformational effect on the homophilic specificity surface may reflect a mechanism by which Ca^{2+} levels regulate the adhesiveness of cad-

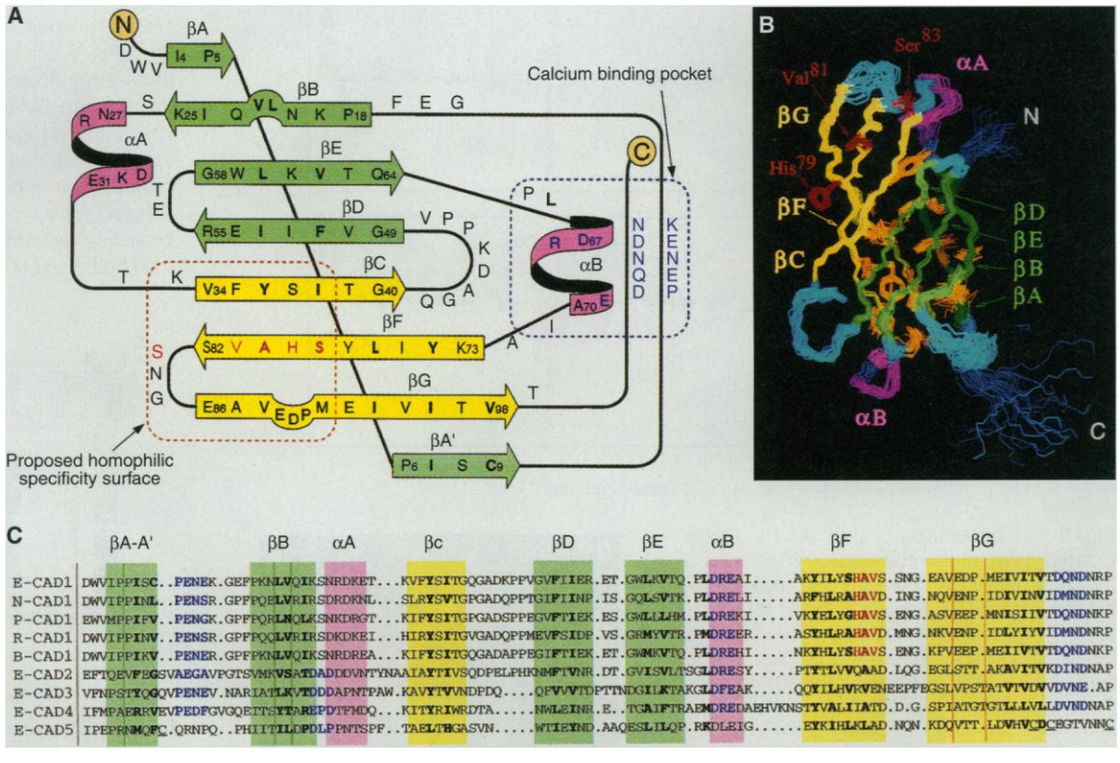

Fig. 1. Structure of the NH_2-terminal CAD domain of E-cadherin (*7*). (**A**) Schematic drawing of the topology with the seven β strands (βA through βG) depicted as arrows and the two α helices (αA and αB) as ribbons. Strands βC, βF, and βG are shown in yellow, the remaining β strands in green, and α helices in magenta. Loops are referred to by the names of the secondary structure elements they join, so that AB refers to the loop between βA and βB. This strand nomenclature is consistent with that of the immunoglobin fold (*9*). The amino acid numbers indicated at the boundary of the secondary structural elements are derived from fully processed E-cadherin (*16*). Blue type indicates amino acids implicated in Ca^{2+} ligation, red type indicates involvement in adhesion (*3, 8*), and bold type indicates buried side chains. The NH_2- and COOH-termini are indicated by N and C. The putative homophilic specificity surface and calcium binding pocket are enclosed in dashed lines. (**B**) Superposition of the backbone heavy atoms (N, Cα, and C) of 20 structures of residues 1 to 104. The color coding is the same as in (A), except that nonregular structure is in blue and heavy atoms of buried side chains are shown in orange. The solvent-exposed side chains of His^{79}, Val^{81}, and Ser^{83} are depicted with their heavy atoms in red. Average root mean square (rms) distributions for backbone and all heavy atoms of amino acids 1 to 100 from the mean structure are 0.66 and 1.09 Å, respectively. The rms deviation from the distance restraints is 0.021 ± 0.0003 Å and from dihedral restraints is 0.60° ± 0.05°. Average rms deviations from idealized geometry used within the program X-PLOR 3.1 (*17*) for bonds, angles, and impropers are 0.009 Å, 2.1°, and 1.1°, respectively. The total, NOE, and Lennard-Jones X-PLOR potential energies are 2487 ± 48, 37.4 ± 5.8, and −158 ± 17 kcal mol^{-1}, respectively (calculated with the use of a square-well potential for the NOE empirical energy term with a force constant of 50 kcal mol^{-1} $Å^{-2}$). (**C**) Structure-based alignment of CAD domain sequences conserving the positions of amino acids that are buried or in turns in mouse E-CAD1. CAD1 domains of mouse neural cadherin (N-CAD1), murine placental cadherin (P-CAD1), chicken retinal cadherin (R-CAD1), chicken brain cadherin (B-CAD1), and mouse E-CAD2, 3, 4, and 5 domains are compared. Secondary structural elements are shown by boxes colored as in (A), with their notation indicated above the boxes. Colored bars indicate junctions or bulges. Calcium-binding sequences are in blue type, HAV motifs of CAD1 domains are red, buried positions are bold, and the four conserved cysteine residues in E-CAD5 are underlined.

herins. Indeed, conservative point mutations within the NH_2-terminal Ca^{2+}-binding pocket abolish adhesion (*11*).

The DAD (*7*) sequence of E-cadherin has been shown to possess Ca^{2+}-binding activity through peptide studies (*11*). Although this sequence is located in the structurally disordered COOH-terminal region of the cadherin polypeptide used here (*5*), the DAD sequence does display substantial Ca^{2+}-dependent chemical shift changes (*12*). This DAD sequence connects βB and αA of E-CAD2 (Fig. 1C). With the use of the crystal structure of the tandem fibronectin type III domains of neuroglian bound to a metal (*13*) as a template, a single Ca^{2+}-binding pocket could be modeled by the βB-αA junction of E-CAD2, AB and αB of CAD1, and the linker between E-CAD1 and E-CAD2 (*12*). Each tandem pair of CAD domains contains these four Ca^{2+}-binding motifs that can form a shared Ca^{2+}-binding pocket (Fig. 3).

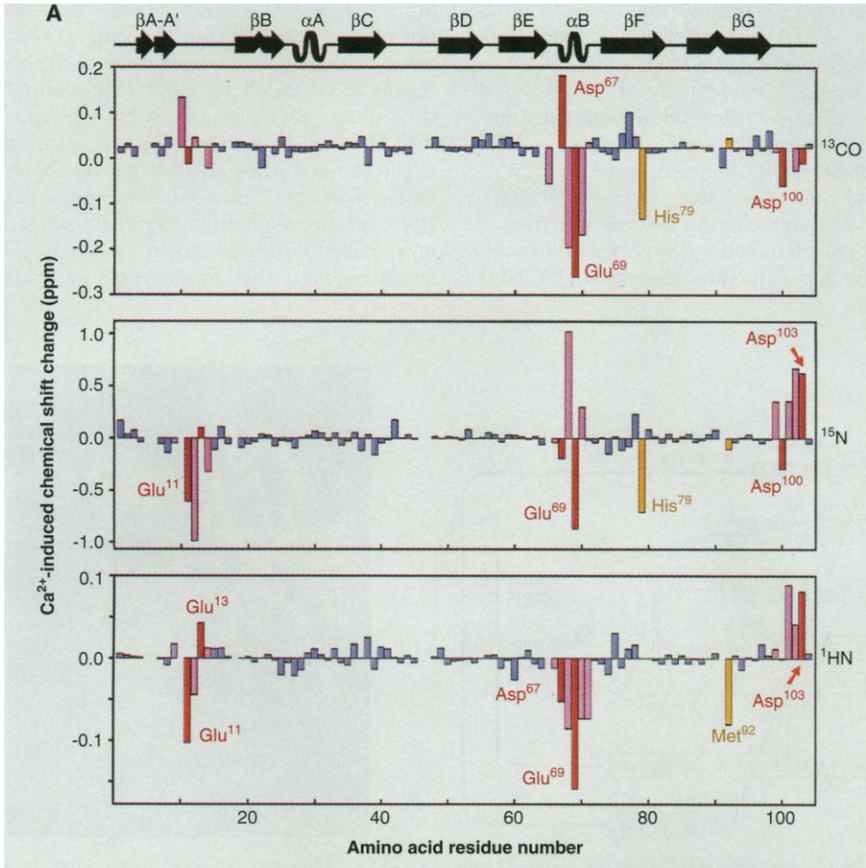

Fig. 2. Calcium-binding pocket. (**A**) The Ca^{2+}-induced chemical shift changes for amino acids 1 to 104 are shown. Amino acids with large chemical shift changes (in parts per million) in the backbone ^{13}CO (top), ^{15}N (middle), and ^{1}HN (bottom) atoms are indicated in red (Asp or Glu), orange (His^{79} and Met^{92}), or magenta (other), whereas those that show only small changes are in blue. The secondary structure elements are indicated above. Chemical shifts were derived from HNCO spectra obtained before and after 10 mM Ca^{2+} was added to 1.5 mM protein (*5*). (**B**) Schematic ribbon drawing of the energy-minimized average E-CAD1 structure showing the side chains of amino acids perturbed by Ca^{2+} binding or implicated in homophilic adhesion. Sidechain heavy atoms of amino acids labeled in (A) are colored as in (A), and the backbone is colored as in Fig. 1B. A possible location of a Ca^{2+} ion equidistant between the sidechain carbonyl groups of Glu^{11}, Glu^{69}, and Asp^{100} is indicated as a blue sphere. The dimensions of the E-CAD1 domain are approximately 22 Å by 22 Å by 42 Å.

Four Ca^{2+}-binding pockets could be formed by the five CAD domains of an E-cadherin molecule. The CAD1 domains of various cadherins do not possess the DAD motif, and CAD5 domains have no PEN, LDRE, and DXND (*7*) motifs (Fig. 1C). This is consistent with the idea that CAD1 and CAD5 each lack one neighbor CAD domain to help coordinate Ca^{2+}. The ligation of Ca^{2+} between tandem CAD domains explains the vulnerability of cadherins to proteolytic degradation when Ca^{2+} is depleted (*1*). Removal of Ca^{2+} would alter the junction between tandem CAD domains and would likely expose the linkers to proteases. The binding of Ca^{2+} at articulation points between CAD domains could provide the rigidity suggested by the Ca^{2+}-induced change of the entire extracellular region of E-cadherin from a globular to a rod-like structure that was observed by electron microscopy (*14*).

The cadherin and Ig CAMs have been considered to constitute distinct superfamilies because of the lack of obvious sequence homology (*1*). However, the E-CAD1 structure reveals marked structural similarities between the two superfamilies. E-CAD1 and probably other CAD domains share similar folding topologies with the extracellular domains of Ig CAMs such as CD2 and CD4 (*9*). The NH_2- and COOH-termini of the extracellular domains of both superfamilies project from opposite ends of the individual β-barrel folds, enabling multiple domains to be strung in tandem (Fig. 3).

The E-CAD1 structure differs from the Ig

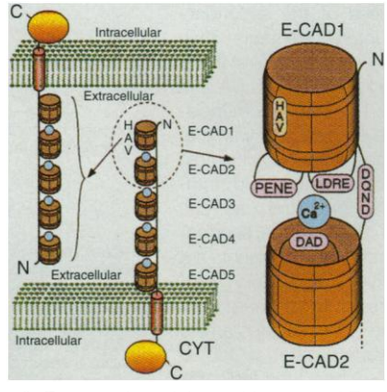

Fig. 3. Proposed modular architecture of E-cadherin (*7*). A schematic drawing of E-cadherin molecules presented by two cells is shown. CAD domains are depicted as brown barrels, cytoplasmic domains (CYT) as yellow-red ellipses, and membrane-spanning regions as pink cylinders. Cell membranes are shown in green. The HAV-containing surfaces on the CAD1 domains contribute to homophilic binding specificity between cadherins, although their binding targets are not yet known. Calcium ions are represented by blue spheres that are sandwiched between tandem CAD domains by the four Ca^{2+}-binding sequences seen in the enlargement of E-CAD1 and E-CAD2 on the right side.

C fold in several ways. The seven β strands of E-CAD1 are all connected by interstrand hydrogen bonds to form an almost completely cylindrical β barrel. The Ig C domain, on the other hand, consists of two distinct β sheets to which additional strands are added to form other variants of the Ig fold (9). The greater twist of the β sheets required to form a cylindrical β barrel results in a more obtuse angle between the directions of the packed β strands in the CAD domain. Thus, the structures of the two domains are virtually nonsuperimposable. The metal binding pocket found in E-CAD1 is absent in the Ig C domain (9), whereas the conserved disulfide bond between βB and βF of the Ig C fold is not present in CAD domains. Membrane-proximal CAD5 domains contain four conserved cysteine residues (Fig. 1C) that may form a disulfide bond or bonds (*15*). In light of the structures of E-CAD1 and an Ig domain in CD2 containing a disulfide bond (9), the first cysteine residue of CAD5 (Fig. 1C) is able to form a disulfide bond with the second or third cysteine of CAD5, thus stabilizing the βA′-βG pairing.

Topological similarities between individual extracellular domains of cadherins and Ig CAMs identified here can be explained either by divergent or convergent evolution. An ancestral CAM domain may have diverged into Ca^{2+}-dependent and Ca^{2+}-independent forms while retaining modular features that are still shared by the cadherin and Ig superfamilies. Alternatively, the independent evolution of analogous extracellular domains by these two superfamilies would attest to the stability and particular suitability of this β-barrel fold for cell-cell adhesion.

REFERENCES AND NOTES

1. M. Takeichi, *Annu. Rev. Biochem.* **59**, 237 (1990); G. M. Edelman and K. L. Crossin, *ibid.* **60**, 155 (1991).
2. M. Takeichi, *Curr. Opin. Cell Biol.* **5**, 806 (1993).
3. A. Nose, K. Tsuji, M. Takeichi, *Cell* **61**, 147 (1990).
4. M. Ozawa *et al.*, *EMBO J.* **8**, 1711 (1989); A. Nagafuchi and M. Takeichi, *Cell Regul.* **1**, 37 (1989).
5. The purification, Ca^{2+}-binding properties, and monomeric state of the recombinant polypeptide comprising amino acids 1 to 144 plus two more NH_2-terminal amino acids of mouse E-cadherin have been described by K. I. Tong *et al.* [*FEBS Lett.* **352**, 318 (1994)]. ^{15}N-labeled, $^{13}C/^{15}N$-labeled, or unlabeled protein was dissolved to 0.5 to 2 mM in either 95% H_2O plus 5% ^2H_2O or 99.996% ^2H_2O containing 100 mM KCl, 10 mM perdeuterated dithiothreitol, 20 mM perdeuterated tris, and 50 μM NaN_3 and 10 mM $CaCl_2$ (except for the Ca^{2+}-free form). Experiments were done on Varian Unity*plus* 500 and Unity 600 spectrometers at 23°C. Most of the NMR-observable ^1H (95.4%), ^{15}N (98.5%), and ^{13}C (88.4%) atoms were assigned by means of the following three-dimensional experiments: ^{15}N-edited total correlation spectroscopy–heteronuclear multiple quantum coherence (TOCSY-HMQC), HNHB, CBCA(CO)NH, HNCACB, H(OCO)NH, HNCO, and HCCH-TOCSY to demonstrate $C\alpha H(i)/C\beta H(i)$-$^{15}N(i)$-$NH(i)$, $C\beta H(i)$-$^{15}N(i)$-$NH(i)$, $^{13}C\beta/C\alpha(i-1)$-$^{15}N(i)$-$NH(i)$, $NH(i)$-$^{15}N(i)$-$^{13}C\beta/C\alpha(i)$, $Hj(i-1)$-$^{15}N(i)$-$NH(i)$, $NH(i)$-$^{15}N(i)$-$^{13}CO(i-1)$, and H_j-$^{13}C_j$-$^{13}C_k$-H_k correlations, respectively (*i* refers to the residue number, whereas *j* and *k* refer to the carbon positions along a side chain). Details of these experiments and original references are provided elsewhere [J. B. Ames, T. Tanaka, L. Stryer, M. Ikura, *Biochemistry* **33**, 10743 (1994); S. Grzesiek, J. Anglister, A. Bax, *J. Magn. Reson.* **101**, 114 (1993)]. Structure calculations used 534 intraresidue, 431 sequential, 161 short-range, and 452 long-range nuclear Overhauser effect (NOE) distances, as well as 87 dihedral and 128 hydrogen bond restraints. The NOE restraints were derived from three dimensional ^{13}C- and ^{15}N-separated NOE spectra [D. R. Muhandiram, N. A. Farrow, G.-Y. Xu, S. H. Smallcombe, L. E. Kay, *J. Magn. Reson.* **102**, 317 (1993); O. Zhang, L. E. Kay, J. P. Oliver, J. D. Forman-Kay, *J. Biomol. NMR* **4**, 845 (1994)] and three-dimensional simultaneous $^{13}C/^{15}N$-separated NOE spectra [S. Pascal, D. R. Muhandiram, T. Yamazaki, J. D. Forman-Kay, L. E. Kay, *J. Magn. Reson.* **101**, 197 (1994)] with 100 ms mixing times, and from two-dimensional homonuclear NOESY spectra with 50 and 200 ms mixing times. The NOEs were classified as 0 to 2.7, 0 to 3.3, and 0 to 5.0 Å on the basis of crosspeak intensity. Val and Leu methyl groups were stereospecifically assigned from the compatibility of rotamer states with NOE intensities. Phi and psi dihedral angle restraints were obtained from coupling constants measured from $^1H/^{15}N$ HMQC-J spectra [L. E. Kay and A. Bax, *J. Magn. Reson.* **86**, 110 (1990)] and from ^{13}C chemical shift indices [D. S. Wishart and B. D. Sykes, *J. Biomol. NMR* **4**, 171 (1993)]. Hydrogen bonds were included as pairs of distance restraints in the final structure calculations based on the identification of slowly exchanging amide hydrogens from $^1H/^{15}N$ HSQC spectra obtained in ^2H_2O and by visual inspection of preliminary structures derived solely from the NOE data. Structure calculations used a simulated annealing protocol [M. Nilges, A. M. Gronenborn, A. T. Brünger, G. M. Clore, *Protein Eng.* **2**, 27 (1988)] in a strategy previously described [S. Bagby, T. S. Harvey, S. G. Eagle, S. Inouye, M. Ikura, *Structure* **2**, 107 (1994)]. Fifty independent structures of amino acids 1 to 104 (the remainder are relatively disordered because of the lack of discernible long-range NOEs and poor chemical shift dispersion) were calculated. Although Ca^{2+} was present in the protein samples, it was not included in the calculations because of the lack of unambiguous NMR constraints.
6. R. J. Poljak *et al.*, *Proc. Natl. Acad. Sci. U.S.A.* **71**, 3440 (1974).
7. Single-letter abbreviations for the amino acid residues are as follows: A, Ala; C, Cys; D, Asp; E, Glu; F, Phe; G, Gly; H, His; I, Ile; K, Lys; L, Leu; M, Met; N, Asn; P, Pro; Q, Gln; R, Arg; S, Ser; T, Thr; V, Val; W, Trp; X, any residue; and Y, Tyr.
8. O. W. Blaschuk, R. Sullivan, S. David, Y. Pouliot, *Dev. Biol.* **139**, 227 (1990).
9. P. Moingeon *et al.*, *Immunol. Rev.* **111**, 111 (1989); E. Y. Jones, *Curr. Opin. Struct. Biol.* **3**, 846 (1993).
10. A. R. Arulanandam *et al.*, *Proc. Natl. Acad. Sci. U.S.A.* **90**, 11613 (1993); C. Somoza, P. C. Driscoll, J. G. Cyster, A. F. Williams, *J. Exp. Med.* **178**, 549 (1993).
11. M. Ozawa, J. Engel, R. Kemler, *Cell* **63**, 1033 (1990).
12. M. Overduin *et al.*, data not shown.
13. A. H. Huber *et al.*, *Neuron* **12**, 717 (1994).
14. S. Pokutta, K. Herrenknecht, R. Kemler, J. Engel, *Eur. J. Biochem.* **223**, 1019 (1994).
15. M. Ozawa *et al.*, *Mech. Dev.* **33**, 49 (1990).
16. A. Nagafuchi *et al.*, *Nature* **329**, 341 (1987); M. Ozawa and R. Kemler, *J. Cell Biol.* **111**, 1645 (1990).
17. A. T. Brünger, *X-PLOR Version 3.1: A System for X-ray Crystallography and NMR* (Yale Univ. Press, New Haven, CT, 1993).

18. We thank L. E. Kay for providing pulse sequences. Supported in part by grants from the Medical Research Council of Canada (MRCC) and the Human Frontier Science Program Organization. M.O., T.S.H., and S.B. thank the National Cancer Institute of Canada, the North Atlantic Treaty Organization, and MRCC, respectively, for postdoctoral fellowships. M.I. holds an MRCC scholarship.

12 October 1994; accepted 21 December 1994

Transcription Factor ATF2 Regulation by the JNK Signal Transduction Pathway

Shashi Gupta, Debra Campbell, Benoit Dérijard, Roger J. Davis*

Treatment of cells with pro-inflammatory cytokines or ultraviolet radiation causes activation of the c-Jun NH_2-terminal protein kinase (JNK). Activating transcription factor–2 (ATF2) was found to be a target of the JNK signal transduction pathway. ATF2 was phosphorylated by JNK on two closely spaced threonine residues within the NH_2-terminal activation domain. The replacement of these phosphorylation sites with alanine inhibited the transcriptional activity of ATF2. These mutations also inhibited ATF2-stimulated gene expression mediated by the retinoblastoma (Rb) tumor suppressor and the adenovirus early region 1A (E1A) oncoprotein. Furthermore, expression of dominant-negative JNK inhibited ATF2 transcriptional activity. Together, these data demonstrate a role for the JNK signal transduction pathway in transcriptional responses mediated by ATF2.

Activating transcription factor–2 [ATF2 (also designated CRE-BP1)] is a member of a group of transcription factors that bind to a similar sequence located in the promoters of many genes (*1*). There has been considerable interest in the role of ATF2 because this transcription factor binds to several viral proteins, including the oncoprotein E1A (*2*, *3*), the hepatitis B virus X protein (*4*), and the human T cell leukemia virus–1 Tax protein (*5*). ATF2 also interacts with the tumor suppressor gene product Rb (*6*), the high mobility group protein HMG I(Y) (*7*), and the transcription factors nuclear factor–κB (NF-κB) (*7*) and c-Jun (*8*). These protein-protein interactions lead to increased transcriptional activity. The function of ATF2 may therefore be determined

S. Gupta and D. Campbell, Program in Molecular Medicine, Department of Biochemistry and Molecular Biology, University of Massachusetts Medical School, Worcester, MA 01605, USA.
B. Dérijard and R. J. Davis, Program in Molecular Medicine and Howard Hughes Medical Institute, University of Massachusetts Medical School, Worcester, MA 01605, USA.
*To whom correspondence should be addressed.